Journal of
Applied Crystallography
ISSN 0021-8898
Editor: **Anke R. Kaysser-Pyzalla**

Particle statistics of a capillary specimen in synchrotron powder diffractometry

T. Ida

J. Appl. Cryst. (2011). **44**, 911–920

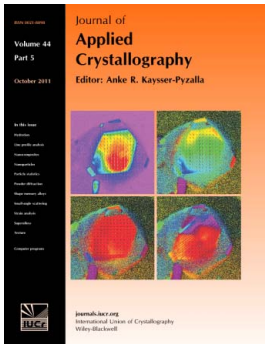

Journal of
Applied Crystallography
ISSN 0021-8898

Received 4 April 2011
Accepted 14 July 2011

Particle statistics of a capillary specimen in synchrotron powder diffractometry

T. Ida

Ceramics Research Laboratory, Nagoya Institute of Technology, Asahigaoka 10-6-29, Tajimi, Gifu 507-0071, Japan. Correspondence e-mail: ida.takashi@nitech.ac.jp

Particle statistics in synchrotron powder diffractometry measured in a capillary transmission mode have been theoretically and experimentally investigated. General mathematical formulae for statistical analysis of observed intensities measured by a spinner-scan method are derived. It is shown that an additional parameter to characterize the size distribution of crystallites can be evaluated from the skewness of the distribution of measured diffraction intensities obtained by the spinner-scan method applied to capillary specimens.

1. Introduction

Analysis of observed powder diffraction intensities generally assumes a sufficiently large number of crystallites that satisfy the diffraction condition. However, it becomes difficult to justify this assumption when the size of crystallites in a powder sample is not small enough and/or the diffractometer has high angular resolution. It is known that the experimental errors caused by particle statistics for a crystalline powder with a particle size of several micrometres are comparable to those caused by counting statistics about intensity data measured under typical experimental conditions (Alexander et al., 1948).

Recently, the author has found that the effect of particle statistics can be evaluated quantitatively by analysis of the diffraction intensities observed by step-scan measurements about the rotation angle of the sample spinner attached to a laboratory powder diffractometer (Ida *et al.*, 2009). It has been concluded that the results of the spinner-scan measurements include information about the texture of the specimen, and evaluation of crystallite sizes of about several micrometres can be achieved by the method, while it is difficult to evaluate crystallite sizes over 0.1 μm by conventional line broadening analysis of a powder diffraction peak profile.

It is expected that the effect of particle statistics will become more pronounced in synchrotron powder diffraction measurements as a result of the high brilliance of synchrotron light sources. On the other hand, higher transparency of the specimen for the tentatively higher energy (shorter wavelength) of synchrotron X-ray photons may reduce the effect of particle statistics owing to the extension of the penetration depth and the effective irradiated volume of specimen.

It is also expected that the axial rotation of a capillary specimen in transmission-mode geometry applicable in synchrotron powder diffractometry will provide more information about the particle statistics than in-plane rotation of a flat specimen. The number of statistically independent data available on the axial rotation of a capillary specimen is estimated at about several tens of thousands, because the angular resolution about the axial rotation is of the order of 0.01°, while in-plane rotation of a flat specimen gives a number of about several hundred, which is restricted by the aspect ratio of the tolerable axial divergence to the equatorial divergence, determined by the geometry of the goniometer.

The skewness of the statistical distribution of the diffraction intensities can be evaluated from such a large number of independent data. This suggests that not only the average size of crystallites but also the broadness of the size distribution can be estimated from a set of diffraction intensity data. Statistical models for size distribution defined by two characteristic parameters, such as lognormal, Gamma or Weibull distributions, can be determined fully by the two characteristic parameters.

Although the fundamental theory of particle statistics about diffraction intensities measured with a laboratory X-ray diffractometer has been established by the pioneering work of Alexander *et al.* (1948) and De Wolff (1958), no practical formulae applicable to the data measured in capillary transmission mode or analysis of crystallite size distribution have been reported. In this study, the author intends to construct a generalized theoretical framework about particle statistics and derive practical mathematical formulae that can be applied to analysis of diffraction intensity data measured with a high-resolution synchrotron powder diffractometer.

2. Theory of particle statistics

In this section, general theoretical formulae for particle statistics are presented. The theoretical framework not only includes the formulae equivalent to those derived by Alexander *et al.* (1948) and De Wolff (1958), but is also extended to discussions about higher-order cumulants of the statistical distribution of the observed diffraction intensities.

It will be shown that the statistical variance of the observed diffraction intensities is determined by the effective number of diffracting crystallites, and the skewness of the statistical

intensity distribution mainly depends on the dispersion of crystallite size distribution in powder specimens.

2.1. Hypothetical case of a non-absorbing sample of uniform particle size

First, a hypothetical situation is formalized, where all the crystallites have the same size and the absorption of the specimen is negligible, similarly to the theoretical work of Alexander *et al.* (1948).

It is assumed that crystallites are randomly oriented in a powder specimen, but it will not be difficult to incorporate the effect of preferred orientation, if necessary.

The reflection multiplicity m is first treated as a unique value for a diffraction peak, and next the effect of overlapping non-equivalent reflections is formalized. The formulae for the effects of the Soller slits that restrict the axial divergence of the diffracted beam and the fundamental resolution function connected with the equatorial divergence are also presented in this section.

2.1.1. Effective number of crystallites and skewness of intensity distribution. The probability ρ that each crystallite contributes to the diffraction intensity of a reflection with multiplicity m is given by

$$\rho = m\Delta\Omega\Delta\mathrm{X}/4\pi, \tag{1}$$

where $\Delta\Omega$ and $\Delta\mathrm{X}$ denote the tolerance angles in the unit of radians for the normal orientation of the diffraction plane to deviate along the equatorial and axial directions, respectively. The product $(\Delta\Omega\Delta\mathrm{X})$ is considered to be a tolerable solid angle, while the whole solid angle is given by 4π.

It has been assumed that $\Delta\Omega$ is restricted by the ratio of the effective focal width of X-ray source to the goniometer radius, and $\Delta\mathrm{X}$ is restricted by the open angle of the Soller slits, in the case of a laboratory Bragg–Brentano diffractometer (Ida *et al.*, 2009). The axial tolerance angle $\Delta\mathrm{X}$ is related to the restriction of the axial divergence of the beam $\Delta\Psi$, by the following equation:

$$\Delta\mathrm{X} = \frac{\Delta\Psi}{2\sin\theta}, \tag{2}$$

for the diffraction angle 2θ. In a typical case of the source width $w_{\mathrm{source}} = 0.1$ mm, goniometer radius $R_{\mathrm{G}} = 185$ mm, axial divergence angle $\Delta\Psi = 2.5^\circ$, diffraction angle $2\theta = 30^\circ$ and multiplicity $m = 2$, the probability is estimated as $\rho \simeq 1.5 \times 10^{-5}$.

It has been suggested that the solid angle of tolerance $(\Delta\Omega\Delta\mathrm{X})$ or an instrumental constant $(\Delta\Omega\Delta\Psi)$ can be calibrated by measurements of powder with known crystallite size distribution (Ida *et al.*, 2009).

It is more difficult to connect each of $\Delta\Omega$ and $\Delta\mathrm{X}$ directly with the optical geometry of a synchrotron beamline and a high-resolution diffractometer with crystal analyser, as compared with the case of a laboratory Bragg–Brentano diffractometer. Hereafter, it is assumed that the parameter $(\Delta\Omega\Delta\Psi)$ can be regarded as an instrumental constant determined by the setup of the synchrotron powder diffraction measurement system. It should be noted that the validity of this assumption is not obvious and should be experimentally examined.

The probability density function $p_j(I_j)$ for the statistical distribution of diffraction intensity I_j from the jth crystallite can be expressed by

$$p_j(I_j) = (1-\rho)\,\delta(I_j) + \rho\,\delta(I_j - I_0), \tag{3}$$

where I_0 is the diffraction intensity from a crystallite satisfying the diffraction condition, and $\delta(x)$ is the Dirac delta function.

The average, variance and third central moment of the diffraction intensity from each crystallite are then given by

$$\langle I_j\rangle = \int_0^\infty I_j p_j(I_j)\,\mathrm{d}I_j = \rho I_0, \tag{4}$$

$$\langle(\Delta I_j)^2\rangle = \rho(1-\rho)I_0^2, \tag{5}$$

$$\langle(\Delta I_j)^3\rangle = \rho(1-\rho)[\rho^2 + (1-\rho)^2]I_0^3. \tag{6}$$

The observed diffraction intensity I is given by

$$I = \sum_{j=1}^{N} I_j, \tag{7}$$

which means that the statistical distribution of the total diffraction intensity I is identical to the multiple convolution of distribution of intensity from each crystallite, that is, the probability density function of the total diffraction intensity $P(I)$ is given by

$$P(I) = \int_0^\infty \cdots \int_0^\infty \delta\left(I - \sum_{j=1}^{N} I_j\right) p_1(I_1)\cdots p_N(I_N)\,\mathrm{d}I_1\cdots\mathrm{d}I_N. \tag{8}$$

Since the cumulant of the convolution is equal to the sum of the cumulants of the component functions, the average, variance and third central moment of the total intensity are exactly given by

$$\langle I\rangle = \int_0^\infty IP(I)\,\mathrm{d}I = N\rho I_0, \tag{9}$$

$$\langle(\Delta I)^2\rangle = N\rho(1-\rho)I_0^2, \tag{10}$$

$$\langle(\Delta I)^3\rangle = N\rho(1-\rho)[\rho^2 + (1-\rho)^2]I_0^3. \tag{11}$$

The effective number of diffracting crystallites N_{eff}, defined as the ratio of the square of the average to the variance of the total intensity I (Alexander *et al.*, 1948), is given by the following equation:

$$N_{\mathrm{eff}} \equiv \frac{\langle I\rangle^2}{\langle(\Delta I)^2\rangle} = \frac{N\rho}{1-\rho} \simeq N\rho, \tag{12}$$

where the last approximation will be justified for $\rho \ll 1$. The quantity N_{eff} can be evaluated experimentally and regarded as the effective number of diffracting crystallites, because it is equal to the expectation value of the number of particles that satisfy the diffraction condition in the case of the non-absorbing sample of uniform crystallite size assumed in this section.

The skewness of the distribution of diffraction intensity expected to be observed for the non-absorbing crystalline powder of uniform particle size is given by

$$S = \frac{\langle(\Delta I)^3\rangle}{\langle(\Delta I)^2\rangle^{3/2}} = \frac{\rho^2 + (1-\rho)^2}{[N\rho(1-\rho)]^{1/2}} \simeq \frac{1}{N_{\rm eff}^{1/2}}, \quad (13)$$

where the last approximation is justified for $\rho \ll 1$ again. The above equation implies that the statistical distribution of the observed diffraction intensity is intrinsically asymmetric, but the asymmetry will be reduced by increasing the number of diffracting crystallites.

2.1.2. Effect of overlapping non-equivalent reflections. The reflection peaks of a Friedel pair always appear at the same position in powder diffractometry, but the component diffraction intensities may not have a common value when there is no inversion centre in the crystallographic symmetry. Other types of systematic overlap of non-equivalent reflections can also be caused by the space-group symmetries. The relative intensities of the 101 and 011 reflections of quartz ($P3_121$ or $P3_221$) are approximately 2:1, for example (Alexander *et al.*, 1948).

The author has introduced the effective multiplicity $m_{\rm eff}$, defined by

$$m_{\rm eff} \equiv \left(\sum_k m_k I_k\right)^2 \left(\sum_k m_k I_k^2\right)^{-1}, \quad (14)$$

for overlapping reflections with component multiplicity m_k and intensity I_k (Ida *et al.*, 2009). The concept of the effective multiplicity certainly simplifies the analytical procedures related to the variance of the observed intensities, because the treatment for overlapping non-equivalent reflections only requires replacement of m by $m_{\rm eff}$ for equivalent reflections. However, this concept should be modified to treat the skewness of the diffraction intensity distribution.

Consider that two groups of non-equivalent reflections of intensities I_1 and I_2 with multiplicity m_1 and m_2 are located at the same peak position. The total probability ρ to satisfy the diffraction condition should be divided into component probability ρ_1 and ρ_2 as follows:

$$\rho = \rho_1 + \rho_2, \quad (15)$$

$$\rho_1 = m_1 \Delta\Omega\Delta{\rm X}/4\pi, \quad (16)$$

$$\rho_2 = m_2 \Delta\Omega\Delta{\rm X}/4\pi. \quad (17)$$

The average, variance and third-order moment of the total intensity are given by

$$\langle I\rangle = N(\rho_1 I_1 + \rho_2 I_2), \quad (18)$$

$$\langle(\Delta I)^2\rangle \simeq N(\rho_1 I_1^2 + \rho_2 I_2^2), \quad (19)$$

$$\langle(\Delta I)^3\rangle \simeq N(\rho_1 I_1^3 + \rho_2 I_2^3). \quad (20)$$

Then the formula of skewness for an overlapping reflection should be modified according to the following formula:

$$S = \frac{\langle(\Delta I)^3\rangle}{\langle(\Delta I)^2\rangle^{3/2}} \simeq \frac{m_{\rm eff}^{1/2}}{(m'_{\rm eff}N_{\rm eff})^{1/2}}, \quad (21)$$

where $m'_{\rm eff}$ is defined by

$$m'_{\rm eff} \equiv (m_1 I_1^2 + m_2 I_2^2)^3 (m_1 I_1^3 + m_2 I_2^3)^{-2}. \quad (22)$$

It is easy to derive a more generalized definition of $m'_{\rm eff}$, given by

$$m'_{\rm eff} \equiv \left(\sum_k m_k I_k^2\right)^3 \left(\sum_k m_k I_k^3\right)^{-2}. \quad (23)$$

Since the effect of reflection multiplicity on the skewness of the observed intensity distribution is generally expressed by the factor $(m_{\rm eff}/m'_{\rm eff})^{1/2}$, it will be omitted in the following discussions about other contributions to observed diffraction intensities.

2.1.3. Effect of Soller slits. It is assumed that the axial (horizontal) divergence of the incident synchrotron X-ray beam is negligible, but the orientation of a diffraction plane in a crystallite is allowed to deviate along the axial direction, this deviation being restricted only by the opening angle of the Soller slits attached on the diffracted-beam side of the high-resolution synchrotron powder diffractometer.

The dependence of the diffracted beam intensity on the axial deviation angle ψ is given by

$$I(\psi) = \begin{cases} (I_0/\Psi)(1 - |\psi|/\Psi) & [|\psi| < \Psi], \\ 0 & [\Psi \le |\psi|], \end{cases} \quad (24)$$

where Ψ is the angle determined by the ratio of the distance to the length of metallic foils in the Soller slits.

The effective axial divergence angle $\Delta\Psi$ is then given by

$$\Delta\Psi = \left[\int_{-\Psi}^{\Psi} I(\psi)\,{\rm d}\psi\right]^2 \left\{\int_{-\Psi}^{\Psi} [I(\psi)]^2\,{\rm d}\psi\right\}^{-1} = 3\Psi/2. \quad (25)$$

The contribution of the Soller slits to the skewness of the intensity distribution is formalized by introducing another parameter, $\Delta\Psi'$, given by

$$\Delta\Psi' \equiv \left\{\int_{-\Psi}^{\Psi} [I(\psi)]^2\,{\rm d}\psi\right\}^3 \left\{\int_{-\Psi_0}^{\Psi_0} [I(\psi)]^3\,{\rm d}\psi\right\}^{-2} = 32\Psi/27. \quad (26)$$

The effect of the Soller slit geometry on the skewness of the observed intensity distribution is expressed by a factor of $(\Delta\Psi/\Delta\Psi')^{1/2} = 9/8 = 1.125$.

2.1.4. Effect of equatorial resolution of the diffractometer. The equatorial deviation of the orientation of a diffraction plane is restricted by the fundamental resolution function, which is affected by the spectroscopic intensity distribution, the equatorial (vertical) divergence of the source X-ray and the diffraction condition at the analyser crystal on the diffracted-beam side of the high-resolution goniometer.

It is assumed that the profile of the resolution function is modelled by the Pearson VII function given by

$$f_{\rm P7}(\omega;\gamma_{\rm P7},\nu) = \frac{\Gamma(\nu)}{\pi^{1/2}\Gamma(\nu - 1/2)} \left(1 + \frac{\omega^2}{\gamma_{\rm P7}^2}\right)^{-\nu}, \quad (27)$$

where γ_{P7} and ν are the width and shape parameters, respectively. $\Gamma(x)$ is the Γ function defined by

$$\Gamma(x) \equiv \int_0^\infty t^{x-1} \exp(-t)\, \mathrm{d}t. \tag{28}$$

The full width at half-maximum (FWHM) of the Pearson VII profile is given by $w_{P7} = 2(2^{1/\nu} - 1)^{1/2}\gamma_{P7}$.

The effective equatorial divergence parameter $\Delta\Omega$ for the Pearson VII profile should be given by

$$\begin{aligned}\Delta\Omega &= \left[\int_{-\infty}^{\infty} f_{P7}(\omega)\, \mathrm{d}\omega\right]^2 \left\{\int_{-\infty}^{\infty} \left[f_{P7}(\omega)\right]^2 \mathrm{d}\omega\right\}^{-1} \\ &= \frac{\pi^{1/2}\Gamma(2\nu)[\Gamma(\nu - 1/2)]^2}{[\Gamma(\nu)]^2\Gamma(2\nu - 1/2)}\gamma_{P7}.\end{aligned} \tag{29}$$

In the Gaussian ($\nu \to \infty$) and Lorentzian ($\nu \to 1$) limits, the values of $\Delta\Omega$ are reduced to $\Delta\Omega(\nu \to \infty) = \pi^{1/2}\gamma_{P7}$ and $\Delta\Omega(\nu \to 1) = 2\pi\gamma_{P7}$.

The modified effective equatorial angle of the Pearson VII profile is then given by

$$\begin{aligned}\Delta\Omega' &\equiv \left\{\int_{-\infty}^{\infty} \left[f_{P7}(\omega)\right]^2 \mathrm{d}\omega\right\}^3 \left\{\int_{-\infty}^{\infty} \left[f_{P7}(\omega)\right]^3 \mathrm{d}\omega\right\}^{-2} \\ &= \frac{\pi^{1/2}[\Gamma(3\nu)]^2[\Gamma(2\nu - 1/2)]^3}{[\Gamma(2\nu)]^3[\Gamma(3\nu - 1/2)]^2}\gamma_{P7},\end{aligned} \tag{30}$$

and the values for the Gaussian and Lorentzian limits are $\Delta\Omega'(\nu \to \infty) = \pi^{1/2}\gamma_{P7}$ and $\Delta\Omega'(\nu \to 1) = 8\pi\gamma_{P7}/9$.

The factor $(\Delta\Omega/\Delta\Omega')^{1/2}$ for the equatorial distribution expressed by the Pearson VII profile is given by

$$\left(\frac{\Delta\Omega}{\Delta\Omega'}\right)^{1/2} = \frac{[\Gamma(2\nu)]^2\Gamma(3\nu - 1/2)\Gamma(\nu - 1/2)}{[\Gamma(2\nu - 1/2)]^2\Gamma(3\nu)\Gamma(\nu)}. \tag{31}$$

When the resolution function is expressed by the Gaussian ($\nu \to \infty$), the skewness of the observed intensity distribution is not changed from that of the uniform distribution, that is, $(\Delta\Omega/\Delta\Omega')^{1/2} = 1$. In the Lorentzian ($\nu = 1$) case, the effect is expressed by $(\Delta\Omega/\Delta\Omega')^{1/2} = 3/2$.

2.2. Effect of absorption in capillary transmission mode

In this section, the effects of absorption in capillary transmission mode upon the observed intensity distribution are formalized.

The diffraction intensity from a crystallite in a cylindrical specimen of linear absorption coefficient μ and radius R is given by

$$\begin{aligned}I_j(r_j, \varphi_j) = I_0 \exp\Big\{&-\mu\left[R^2 - r_j^2 \sin^2(\varphi_j + \theta)\right]^{1/2} \\ &- \mu\left[R^2 - r_j^2 \sin^2(\varphi_j - \theta)\right]^{1/2}\Big\} \\ &\times \exp\left(-2\mu r_j \sin\theta \sin\varphi_j\right),\end{aligned} \tag{32}$$

when the crystallite is located at the position $(x_j, y_j) = (r_j \cos\varphi_j, r_j \sin\varphi_j)$ in a coordinate system with the origin on the centre of the cylinder.

Table 1
Overall transmittance $A(\mu R, \theta)$ and modification factors f_{cap}, g_{cap} for a cylinder of $\mu R = 0.5$.

2θ (°)	0	30	60	90	120	150
$A(\mu R, \theta)$	0.435	0.438	0.446	0.459	0.473	0.484
f_{cap}	0.963	0.946	0.906	0.865	0.833	0.814
g_{cap}	1.049	1.075	1.120	1.146	1.152	1.152

Since the overall transmittance $A(\mu R, \theta)$ of a cylinder, related to the absorption correction factor $A^*(\mu R, \theta)$ as $A(\mu R, \theta) = 1/A^*(\mu R, \theta)$, is given by (Dwiggins, 1975)

$$\begin{aligned}A(\mu R, \theta) = \frac{2}{\pi R^2}\int_{-\pi/2}^{\pi/2}\int_0^R r \exp\Big\{&-\mu\left[R^2 - r^2 \sin^2(\varphi + \theta)\right]^{1/2} \\ &- \mu\left[R^2 - r^2 \sin^2(\varphi - \theta)\right]^{1/2}\Big\} \\ &\times \exp\left(-2\mu r \sin\theta \sin\varphi\right) \mathrm{d}r\, \mathrm{d}\varphi,\end{aligned} \tag{33}$$

the average of the kth power of the diffraction intensity from a crystallite is generally given by

$$\langle I_j^k \rangle = I_0^k A(k\mu R, \theta). \tag{34}$$

Therefore, the effective number of diffracting crystallites N_{eff} should be modified by the factor of

$$f_{cap}(\mu R, \theta) = [A(\mu R, \theta)]^2 / A(2\mu R, \theta), \tag{35}$$

the value of which lies in the range $0 < f_{cap}(\mu R, \theta) < 1$. This implies that the absorption by the specimen not only reduces the irradiated volume but also causes additional variation in measured diffraction intensities.

A modified factor given by

$$f'_{cap}(\mu R, \theta) = [A(2\mu R, \theta)]^3 / [A(3\mu R, \theta)]^2 \tag{36}$$

is introduced in a similar way to the formulations given in §2.1. The skewness should then be modified by the factor of

$$g_{cap}(\mu R, \theta) = \left[\frac{f_{cap}(\mu R, \theta)}{f'_{cap}(\mu R, \theta)}\right]^{1/2} = \frac{A(3\mu R, \theta)\, A(\mu R, \theta)}{[A(2\mu R, \theta)]^2}. \tag{37}$$

Table 1 lists the values of overall transmittance $A(\mu R, \theta)$, and factors f_{cap} and g_{cap} calculated for a cylinder of $\mu R = 0.5$ and diffraction angles $2\theta = 0, 30, \ldots, 150°$. The function $A(\mu R, \theta)$ can be evaluated efficiently by a method recently developed by the author (Ida, 2010).

It should be noted that the distribution of the observed diffraction intensities should certainly be affected by the absorption, but the difference from the non-absorbing case is not very large in the case of $\mu R = 0.5$.

2.3. Effect of particle size distribution

It is assumed that the statistical distribution of the volume v_j of a crystallite is expressed by a probability density function $p_{size}(v_j)$. Since the diffraction intensity from a crystallite is proportional to the particle volume, the probability density function for the diffraction intensity from a crystallite is given by

$$p_j(I_j) = (1-\rho)\,\delta(I_j) + \rho\int_0^\infty \delta(I_j - I_v v_j)\,p_{\rm size}(v_j)\,{\rm d}v_j$$
$$= (1-\rho)\,\delta(I_j) + \rho\,p_{\rm size}(I_j/I_v)/I_v, \qquad (38)$$

where I_v is the diffraction intensity per unit volume.

The statistical average, variance and third central moment of the intensity from a crystallite are then given by

$$\langle I_j\rangle = \int_0^\infty I_j p_j(I_j)\,{\rm d}I_j = \rho I_v\langle v_j\rangle, \qquad (39)$$

$$\langle(\Delta I_j)^2\rangle = \rho I_v^2\big(\langle v_j^2\rangle - \rho\langle v_j\rangle^2\big), \qquad (40)$$

$$\langle(\Delta I_j)^3\rangle = \rho I_v^3\big[\langle v_j^3\rangle - 3\rho\langle v_j^2\rangle\langle v_j\rangle + 2\rho^2(2-\rho)\langle v_j\rangle^3\big], \qquad (41)$$

where $\langle v_j\rangle$, $\langle v_j^2\rangle$ and $\langle v_j^3\rangle$ are the average, squared and cubic averages of the particle volume, respectively, which are defined by the following common formula:

$$\langle v_j^k\rangle \equiv \int_0^\infty v_j^k p_{\rm size}(v_j)\,{\rm d}v_j. \qquad (42)$$

The effective number of diffracting crystallites for a non-absorbing sample is given by

$$N_{\rm eff} = \frac{N\rho\langle v_j\rangle^2}{\langle v_j^2\rangle - \rho\langle v_j\rangle^2} \simeq \frac{N\rho\langle v_j\rangle^2}{\langle v_j^2\rangle}, \qquad (43)$$

where the approximation holds for small ρ. The above equation can be rewritten as

$$N_{\rm eff} \simeq \frac{f V\rho\langle v_j\rangle}{\langle v_j^2\rangle}, \qquad (44)$$

for the irradiated volume V and filling factor of powder f, because the number of particles is given by $N = fV/\langle v_j\rangle$. This means that the effective number of diffracting crystallites of any size distribution is equivalent to the case of uniform particle volume of $\langle v_j^2\rangle/\langle v_j\rangle$.

The filling factor f relates the linear absorption coefficients of the powder specimen μ and bulk material μ_0 by $\mu = f\mu_0$.

The skewness of the statistical distribution of the diffraction intensity is given by

$$S = \frac{\langle v_j^3\rangle - 3\rho\langle v_j^2\rangle\langle v_j\rangle + 2\rho^2\langle v_j\rangle^3}{(N\rho)^{1/2}\big(\langle v_j^2\rangle - \rho\langle v_j\rangle^2\big)^{3/2}} \simeq \frac{\langle v\rangle}{(N\rho)^{1/2}\langle v\rangle^{3/2}}. \qquad (45)$$

It is related to the effective number of diffracting crystallites by the following equation:

$$S \simeq \frac{\langle v_j^3\rangle\langle v_j\rangle}{N_{\rm eff}^{1/2}\langle v_j^2\rangle^2}, \qquad (46)$$

which means that the skewness should be varied proportionally to the value $\langle v_j^3\rangle\langle v_j\rangle/\langle v_j^2\rangle^2$, even if the effective number of diffracting crystallites $N_{\rm eff}$ is unchanged.

The density function of lognormal distribution for the particle diameter D_j is given by

$$p_{\rm LN}(D_j) \equiv \frac{1}{(2\pi)^{1/2}\omega D_j}\exp\left[-\frac{1}{2\omega^2}\left(\ln\frac{D_j}{D_{\rm m}}\right)^2\right], \qquad (47)$$

where $D_{\rm m}$ is the median diameter and ω is the logarithmic standard deviation. When the particles are assumed to have spherical shape, the average of the kth power of the particle volume is given by

$$\langle v_j^k\rangle = \big(\pi D_{\rm m}^3/6\big)^k\exp\big(9k^2\omega^2/2\big). \qquad (48)$$

The effective particle volume $v_{\rm eff}$ and diameter $D_{\rm eff}$ for particle statistics and the modification factor $\kappa_{\rm eff}$ for the skewness of intensity distributions are given by

$$v_{\rm eff} \equiv \langle v_j^2\rangle/\langle v_j\rangle = (\pi D_{\rm m}^3/6)\exp\big(27\omega^2/2\big), \qquad (49)$$

$$D_{\rm eff} \equiv (6v_{\rm eff}/\pi)^{1/3} = D_{\rm m}\exp\big(9\omega^2/2\big), \qquad (50)$$

$$\kappa_{\rm eff} \equiv \langle v_j^3\rangle\langle v_j\rangle/\langle v_j^2\rangle^2 = \exp(9\omega^2). \qquad (51)$$

It will not be difficult to derive formulae for nonspherical shapes and/or another model for size distribution, if an appropriate model is available.

2.4. Combined formulae for particle statistics

Finally, the combined formulae for the effective number of diffracting crystallites $(N_{\rm eff})_{\rm cap}$ and the skewness of the intensity distribution $S_{\rm cap}$ measured in a capillary transmission mode are presented in this section.

The effective number of diffracting crystallites is given by

$$(N_{\rm eff})_{\rm cap} = \frac{\pi\rho_{\rm eff}\mu R^2 L\langle v_j\rangle[A(\mu R,\theta)]^2}{\mu_0\langle v_j^2\rangle A(2\mu R,\theta)}, \qquad (52)$$

where μ and μ_0 are the linear absorption coefficients of the powder specimen and bulk material, respectively, R is the radius of the capillary, L is the width of the cross section of the X-ray beam along the axial direction, and the function $A(\mu R,\theta)$ is the transmission coefficient of the capillary at the Bragg angle θ. The parameter $\rho_{\rm eff}$ is the effective probability that each crystallite satisfies the diffraction condition, given by

$$\rho_{\rm eff} = \frac{m_{\rm eff}\Delta\Omega\Delta\Psi}{8\pi\sin\theta}, \qquad (53)$$

for the effective multiplicity $m_{\rm eff}$ and the allowed deviation angles along the axial and equatorial directions, $\Delta\Psi$ and $\Delta\Omega$, respectively. The formulae for $m_{\rm eff}$, $\Delta\Psi$ and $\Delta\Omega$ have been given in equations (14), (25) and (29). The definition of $\langle v_j^k\rangle$ is given by equation (42).

The skewness of the intensity distribution is given by

$$S_{\rm cap} = \frac{(m_{\rm eff}\Delta\Omega\Delta\Psi)^{1/2}\langle v_j^3\rangle\langle v_j\rangle A(3\mu R,\theta)\,A(\mu R,\theta)}{[(N_{\rm eff})_{\rm cap}m'_{\rm eff}\Delta\Omega'\Delta\Psi']^{1/2}\langle v_j^2\rangle^2[A(2\mu R,\theta)]^2}, \qquad (54)$$

where $m'_{\rm eff}$, $\Delta\Psi'$ and $\Delta\Omega'$ are the parameters given by equations (23), (26) and (30), respectively.

3. Experimental

3.1. Powder samples

Three fractions of quartz powder separated by a sedimentation method were used without further grinding or

Table 2
Parameters of size distribution evaluated by SEM image analysis of three fractions of quartz powder separated by a sedimentation method.

Stokes diameter (μm)	3–7	8–12	18–22
$D_{\rm m}$ (μm)	4.831 (6)	9.239 (18)	21.03 (2)
ω	0.2836 (11)	0.2400 (12)	0.1937 (11)
$D_{\rm eff}$ (μm)	7.0	12.0	28
$\kappa_{\rm eff}$	2.06	1.68	1.40

sieving. The nominal Stokes diameters of the fractions were 3–7, 8–12 and 18–22 μm. The crystallite size distributions of the fractions were determined by analysis of scanning electron microscopy (SEM) images (Ida *et al.*, 2009). The characteristic parameters for the optimized lognormal distributions are listed in Table 2. The effective diameter $D_{\rm eff}$ is calculated by $D_{\rm eff} = (6v_{\rm eff}/\pi)^{1/3}$ from the effective particle volume $v_{\rm eff}$.

Three powder samples (1, 2 and 3) with similar averages and different degrees of dispersion about the size distribution were prepared as controlled mixtures of the separated fractions. The effective particle diameter $D_{\rm eff}$ and modification factor $\kappa_{\rm eff} = \langle v_j^3\rangle\langle v_j\rangle/\langle v_j^2\rangle^2$ for the mixture are calculated by

$$D_{\rm eff} = \left[\sum_n w_n (D_{\rm m})_n^3 \exp(27\omega_n^2/2)\right]^{1/3}, \tag{55}$$

$$\kappa_{\rm eff} = \frac{\sum_n w_n (D_{\rm m})_n^6 \exp(36\omega_n^2)}{\left[\sum_n w_n (D_{\rm m})_n^3 \exp(27\omega_n^2/2)\right]^2}, \tag{56}$$

where w_n, $(D_{\rm m})_n$ and ω_n are the weight fraction, median diameter and logarithmic standard deviation of the nth component, respectively. The weight fractions and calculated values of $D_{\rm eff}$ and $\kappa_{\rm eff}$ are listed in Table 3.

The three powder samples 1, 2 and 3 were filled into Lindemann glass capillaries with a nominal diameter of 0.5 mm.

3.2. Measurements

A high-resolution synchrotron powder diffractometer equipped with a flat Ge(111) crystal analyser on the beamline BL4B2 at the Photon Factory in Tsukuba was used for diffraction measurements. The peak wavelength of the source X-ray beam calibrated with the peak positions of a standard Si powder (NIST SRM640c) was 1.20670 (3) Å.

The transmittance intensity profile was recorded by scanning the vertical position of the capillary samples at the step interval of 0.01 mm. The cross section of the incident beam was restricted to be 0.05 mm along the vertical direction with the entrance slit of the diffractometer.

The observed intensity profile $I(z)$ was fitted by the following model:

$$I(z) = I_1(z) * I_2(z), \tag{57}$$

$$I_1(z) = \begin{cases} I_0 \exp\{-2\mu[R^2 - (z - z_0)^2]^{1/2}\} & \text{for} \quad |z - z_0| < R, \\ I_0 & \text{for} \quad R \le |z - z_0|, \end{cases} \tag{58}$$

Table 3
Mixing ratio and parameters of size distribution for three samples of quartz powder.

w(3–7), w(8–12) and w(18–22) are the weight fractions of component powders with the nominal Stokes diameter 3–7, 8–12 and 18–22 μm, respectively.

Sample	1	2	3
w(3–7) (%)	0	54.2	92.6
w(8–12) (%)	100	42.2	0
w(18–22) (%)	0	3.6	7.4
$D_{\rm eff}$ (μm)	12.0	11.3	11.3
$\kappa_{\rm eff}$	1.68	6.67	11.8

Table 4
Characteristic parameters of capillary specimens.

$2R$ is the diameter of the capillary, μ is the linear absorption coefficient, and $f_{\rm cap}$(101/011) and $g_{\rm cap}$(101/011) are the modification factors for the 101/011 reflection of quartz at the diffraction angle $2\theta = 20.625^\circ$.

Sample	1	2	3
$2R$ (mm)	0.575 (1)	0.547 (1)	0.508 (1)
μ (cm^{-1})	17.11 (9)	17.34 (8)	15.50 (8)
μR	0.492	0.474	0.394
$f_{\rm cap}$(101/011)	0.970	0.972	0.982
$g_{\rm cap}$(101/011)	1.060	1.054	1.034

$$I_2(z) = \begin{cases} 1/H & \text{for} \quad |z| < H/2, \\ 0 & \text{for} \quad H/2 \le |z|, \end{cases} \tag{59}$$

where I_0 is the intensity of the incident beam, R the radius of the capillary, z_0 the centre position and H the height of the cross section of the incident beam, restricted by the entrance slit.

The results of fitting for the intensity profile of sample 1 are shown in Fig. 1, and the values of optimized parameters for the three capillary specimens are listed in Table 4. The values of modification factors $f_{\rm cap}$ and $g_{\rm cap}$ for cylindrical samples, calculated for the 101/011 reflection of quartz at the diffraction angle $2\theta = 20.625^\circ$, are also listed in Table 4.

The 2Θ scan peak profiles of the quartz 101/011 reflection were recorded for capillary specimens 1, 2 and 3. The step interval was 0.01° in 2Θ, and the measurement time was 0.5 s

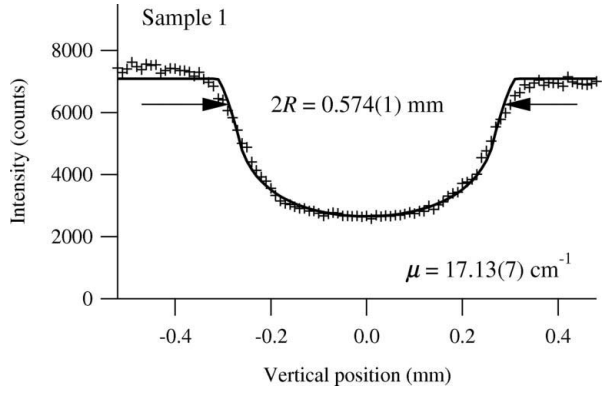

Figure 1
Intensity profile on a vertical scan of capillary specimen 1. The observed intensities are marked by crosses, and the fitted curve is drawn as a solid line.

per step. The capillary specimens were continuously rotated at a speed of 2 r s^{-1} during the measurements.

Five thousand peak-top intensities of the quartz 101/011 reflection were recorded for each sample on stepwise rotation of the capillary specimens over 360° at an interval of 0.072°.

4. Results and discussions

4.1. Peak profile

Fig. 2 shows the 2Θ scan peak profiles of the 101/011 reflection of the quartz powder specimens 1, 2 and 3. The observed profiles were fitted by the convolution of the Pearson VII profile $f_{\rm P7}(x;\gamma_{\rm P7},\nu)$ shown in equation (27) and the axial-divergence aberration function $w_{\rm A}(x;\Psi)$ (Ida & Hibino, 2006). The formula of the fitting function $p_{\rm P7*A}(2\Theta)$ is given by

$$p_{\rm P7*A}(2\Theta) = b + If_{\rm P7}(2\Theta - 2\theta;\gamma_{\rm P7},\nu) * w_{\rm A}(2\Theta;\Psi), \quad (60)$$

$$w_{\rm A}(x;\Psi) = \begin{cases} |\beta_{\rm A}|^{-1}[(-x/\beta_{\rm A})^{-1/2} - 1] & \text{for } -1 < x/\beta_{\rm A} < 0, \\ 0 & \text{elsewhere,} \end{cases} \quad (61)$$

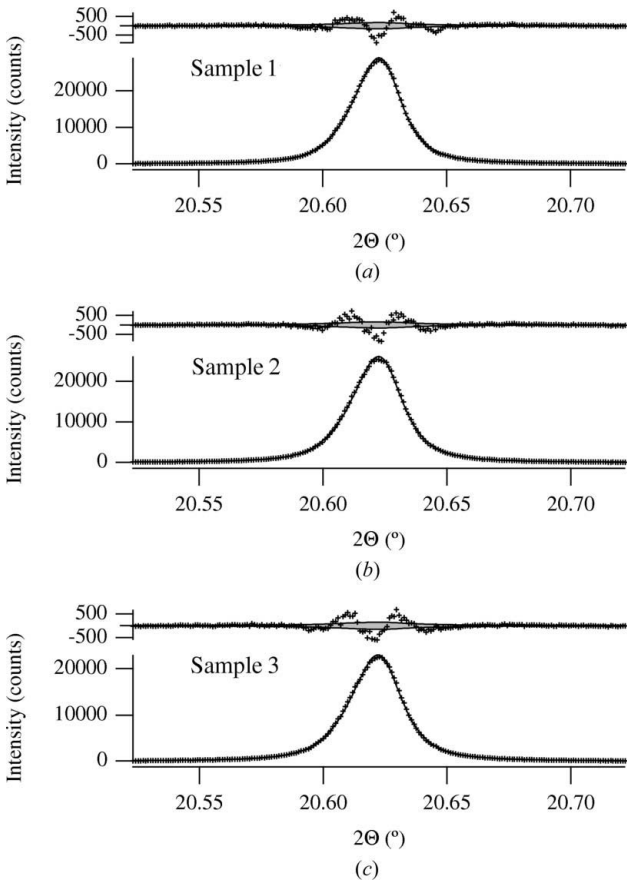

Figure 2
The 2Θ diffraction profiles of the 101/011 reflection of quartz powder samples (*a*) 1, (*b*) 2 and (*c*) 3. The observed intensities are marked by crosses, and the fitted curves are drawn as solid lines in the lower panels. The upper panels show the difference plots (crosses) and errors predicted by counting statistics (grey area).

Table 5
Optimized parameters of profile fitting.

b is the constant background, *I* is the integrated intensity, 2θ is the peak location, and $w_{\rm P7}$ and ν are the FWHM and shape parameters of the symmetric Pearson VII function. The errors estimated for 2θ and $w_{\rm P7}$ are omitted, because they are smaller than the mechanical precision of about 0.0001°.

Sample	1	2	3
b	143 (3)	143 (4)	143 (4)
I	828 (2)	784 (2)	703 (2)
2θ (°)	20.6255	20.6253	20.6248
$w_{\rm P7}$ (°)	0.0190	0.0201	0.0205
ν	1.480 (9)	1.453 (9)	1.432 (10)

$$\beta_{\rm A} = (\Psi^2/2)(\cot 2\theta + \tan\Theta_{\rm A}), \quad (62)$$

where *b* is the constant background, *I* the integrated intensity and $\Theta_{\rm A}$ the Bragg angle of the analyser crystal.

The optimized values of fitting parameters are listed in Table 5. The smaller values of the shape parameter ν for the samples with broader size distribution may be related to the theories (Langford *et al.*, 2000; Popa & Balzar, 2002; Ida *et al.*, 2003) that predict that the intrinsic diffraction peak profile from small crystallites becomes more 'Lorentzian-like' for a more dispersed crystallite size distribution.

The effects on the equatorial intensity distribution as calculated by equation (31) are $(\Delta\Omega/\Delta\Omega')^{1/2} = 1.321$, 1.326 and 1.330 for samples 1, 2 and 3, respectively.

4.2. Spinner-scan data

The spinner-scan intensity profiles measured for samples 1, 2 and 3 are shown in Fig. 3. The statistical independence of the data is supported by the lack of systematic variation in the observed intensity profiles. Evolution of asymmetry in the statistical distribution of the observed diffraction intensities for samples with more dispersed particle size distribution can be viewed directly in the profile in Fig. 3. The histograms of the observed intensities are shown in Fig. 4.

The average, variance, third-order central moment and skewness of the observed intensity distributions are listed in Table 6. The errors in parentheses are estimated from the higher-order central moments of the observed data (see Appendix *A*).

The estimated relative error of the average is equal to $1/(NN_{\rm eff})^{1/2}$, which is expected for a Poisson distribution with the expectation value of $N_{\rm eff}$ by definition. The relative errors of the variance estimated at 0.032, 0.040 and 0.062 for samples 1, 2 and 3 are of the same order as the value $2/N^{1/2} = 0.028$ expected for a Poisson distribution. The relative errors for the third-order moment estimated at 0.16, 0.15 and 0.15 for samples 1, 2 and 3 are also of the same order as the values $(6N_{\rm eff}/N)^{1/2}$ = 0.28, 0.30 and 0.26, respectively. The resemblance of the observed statistics to the Poisson distribution with the expected value of $N_{\rm eff}$ suggests that the variation of the measured diffraction intensities is certainly dominated by the finite number of diffracting crystallites.

The effective multiplicities of the quartz 101/011 reflection are estimated at $m_{\rm eff} = 10.27$ and $m'_{\rm eff} = 8.45$ from the

Table 6
Characteristics of spinner-scan data.

The value of the effective diameter $D_{\rm eff}$ of sample 1 estimated by SEM image analysis is treated as the reference to determine the instrumental constant.

Sample	1	2	3
$\langle I\rangle$	28370 (50)	25430 (40)	22380 (40)
$\langle(\Delta I)^2\rangle$	1.29 (4) $\times 10^7$	8.7 (4) $\times 10^6$	8.8 (5) $\times 10^6$
$\langle(\Delta I)^3\rangle$	2.6 (4) $\times 10^{10}$	3.1 (5) $\times 10^{10}$	7.5 (11) $\times 10^{10}$
S	0.56 (9)	1.22 (19)	2.9 (5)
$N_{\rm eff}$	62 (3)	74 (5)	56 (6)
$D_{\rm eff}$ (μm)	12.0 (fixed)	11.0 (7)	11.1 (1.2)
$\kappa_{\rm eff}$	2.8 (5)	6.7 (1.0)	14 (2)

component multiplicities $m_{101} = m_{011} = 6$ and the calculated relative intensities of $I_{011}/I_{101} = 2.393$ obtained by the preliminary Rietveld analysis using RIETAN-FP developed by Izumi & Momma (2007).

The effective crystallite diameter of sample 1 estimated at $D_{\rm eff} = 12.0$ μm by the SEM image analysis is treated as the reference value to calibrate the instrumental constant in this study. The effective equatorial tolerance angle is estimated at $\Delta X = 0.061\ (2)^\circ$ from the effective number of diffracting crystallites $N_{\rm eff} = 62\ (3)$ evaluated from the spinner-scan data, assuming $\mu R = 0.492$, $R = 0.288$ mm, $[A(\mu R, \theta)]^2/A(2\mu R, \theta) = 0.970$, $\mu/\mu_0 = 17.11/48.49 = 0.3529$, $L = 10$ mm and $\Delta\Psi = 1.5^\circ$

The effective diameters of samples 2 and 3 listed in Table 6 are evaluated from the observed average and variance of the spinner-scan data and the instrumental constants. The values coincide with those estimated from the SEM image analysis listed in Table 3 within the estimated experimental errors.

The crystallite size dispersion parameters $\kappa_{\rm eff}$ evaluated for samples 1, 2 and 3 by statistical analysis of the observed spinner-scan data are listed in the last row of Table 6. Good agreement with the values estimated by the SEM image analysis have been found, except that the value of $\kappa_{\rm eff}$ determined for sample 1 by the spinner-scan method is slightly larger than that predicted by the SEM image analysis.

The relative errors of the skewness estimated for samples 1, 2 and 3 are 0.16, 0.16 and 0.17, while those predicted for the Poisson case (see Appendix *A*4) for $N = 5000$ are about 0.3.

The area-weighted average diameter defined by $\langle D\rangle_{\rm A} \equiv \langle D^3\rangle/\langle D^2\rangle$ can be connected with the experimentally obtained values of $D_{\rm eff}$ and $\kappa_{\rm eff}$ by the equation $\langle D\rangle_{\rm A} = D_{\rm eff}\kappa_{\rm eff}^{-2/9}$, when the lognormal distribution is assumed. The values of $\langle D\rangle_{\rm A}$ for samples 1, 2 and 3 are then estimated at 9.5 (8), 7.2 (7) and 6.2 (8) μm, while the values calculated from the mixing ratios w_j and the parameters $D_{\rm m}$ and ω for each

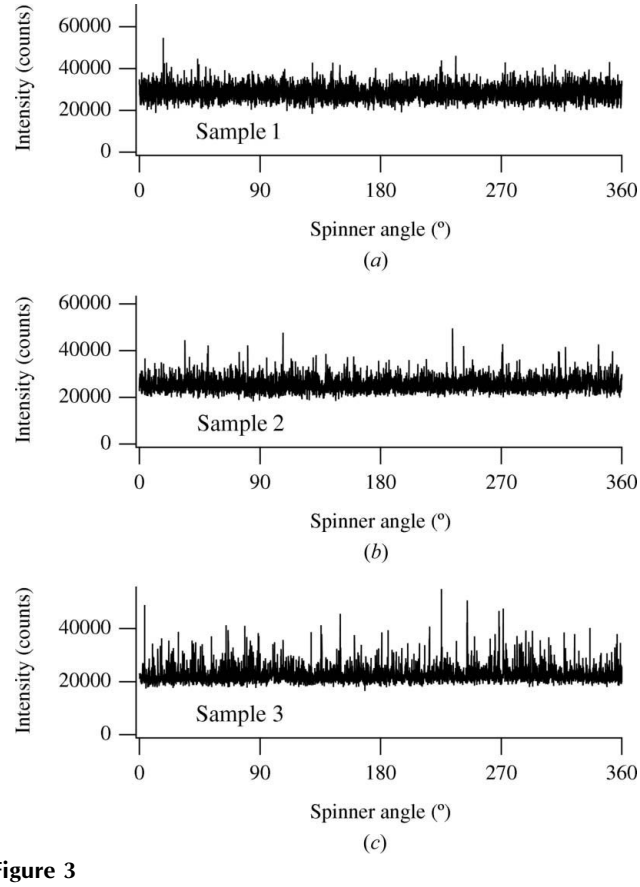

Figure 3
The spinner-scan profiles of the 101/011 reflection of quartz powder samples (*a*) 1, (*b*) 2 and (*c*) 3. The observed intensities are drawn as solid lines.

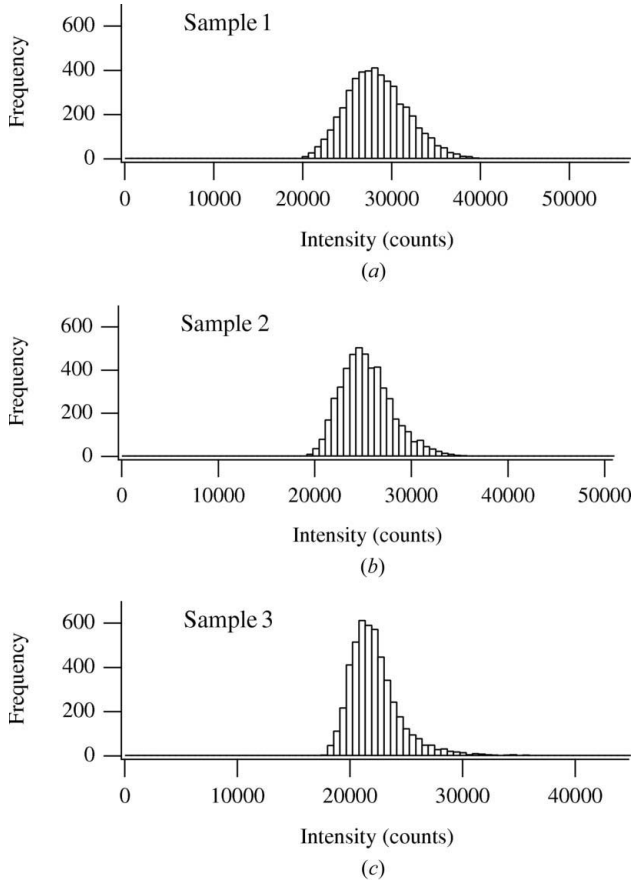

Figure 4
The histograms of the 101/011 reflection intensity distribution of quartz powder samples (*a*) 1, (*b*) 2 and (*c*) 3.

fraction determined from the SEM image analysis are 10.7, 7.5 and 6.3 μm.

5. Conclusion

Observed powder diffraction intensities are considered to be the multiple convolution of the diffraction from each crystallite. Quantitative descriptions of the statistical properties of the observed intensities have been derived on the basis of the additivity of cumulants with respect to convolution.

Practical formulae for the particle statistics of capillary specimens in synchrotron powder diffractometry are presented. The skewness of the observed intensity distribution is predominantly affected by a size dispersion parameter, which can be connected with the broadness of the crystallite size distribution.

The errors in the experimentally estimated skewness were evaluated by utilizing the sample central moments up to sixth order. The experimental values of skewness evaluated from collections of diffraction intensity data measured by a spinner-scan method agree well with the values predicted from the results of SEM image analysis.

APPENDIX *A*
Estimation of cumulants up to the third order

A1. Cumulants

The kth-order cumulant κ_k for a probability density function $p(x)$ is defined by

$$\kappa_k \equiv \lim_{\theta\to 0} \frac{\partial^k}{\partial \theta^k} \ln \int_{-\infty}^{\infty} \exp(\theta x)\, p(x)\, \mathrm{d}x, \tag{63}$$

while the kth-order central moment μ_κ is defined by

$$\mu_k \equiv \int_{-\infty}^{\infty} (x-\overline{x})^k p(x)\, \mathrm{d}x, \tag{64}$$

where $\overline{x}$ is the average given by

$$\overline{x} \equiv \int_{-\infty}^{\infty} x\, p(x)\, \mathrm{d}x. \tag{65}$$

The first, second and third-order cumulants are equivalent to the mean $\overline{x}$, the variance σ^2 and the third-order central moment μ_3, that is, $\kappa_1 = \overline{x}$, $\kappa_2 = \mu_2 = \sigma^2$, $\kappa_3 = \mu_3$. The cumulants from the fourth to sixth order are related to the central moments μ_k by $\kappa_4 = \mu_4 - 3\mu_2^2$, $\kappa_5 = \mu_5 - 10\mu_3\mu_2$ and $\kappa_6 = \mu_6 - 15\mu_4\mu_2 - 10\mu_3^2 + 30\mu_2^3$.

A2. Unbiased estimation

Consider N independent sample data $\{X_j\}$ $(j = 0, \ldots, N-1)$ about a stochastic variable with the mean $\overline{x}$, variance σ^2 and third-order cumulant κ_3. The sample average is defined by

$$\overline{X} \equiv N^{-1} \sum_{j=0}^{N-1} X_j, \tag{66}$$

and the expected value of $\overline{X}$ coincides with the true mean value, that is, $\langle \overline{X} \rangle = \overline{x}$.

The unbiased estimation of the variance is given by

$$V = N(N-1)^{-1} M_2, \tag{67}$$

where M_k is the kth-order sample central moment defined by

$$M_k \equiv N^{-1} \sum_{j=0}^{N-1} (X_j - \overline{X})^k. \tag{68}$$

Note that the above formula for the unbiased sample variance is determined to satisfy that the expected value of V should be equal to σ^2, that is, $\langle V \rangle = \sigma^2$.

The unbiased estimation of the third-order cumulant is similarly given by

$$T = N^2(N-1)^{-1}(N-2)^{-1} M_3, \tag{69}$$

so that $\langle T \rangle = \kappa_3$.

A3. Errors in estimation of statistical parameters

The statistical variance of the sample average $\overline{X}$ is given by

$$(\Delta \overline{X})^2 \equiv \langle (\overline{X} - \overline{x})^2 \rangle = \sigma^2/N \simeq M_2/N. \tag{70}$$

The statistical variance about the unbiased sample variance V calculated by equation (67) can be estimated as the expected value of the squared difference of V from the true variance σ^2, which is approximated by

$$(\Delta V)^2 \equiv \langle (V - \sigma^2)^2 \rangle \simeq (M_4 - M_2^2)/N. \tag{71}$$

The statistical variance of the unbiased third-order cumulant T calculated by equation (69) is similarly approximated by

$$\begin{aligned} (\Delta T)^2 &\equiv \langle (T - \kappa_3)^2 \rangle \\ &\simeq (M_6 - 6M_4M_2 - M_3^2 + 9M_2^3)/N. \end{aligned} \tag{72}$$

The variance in the estimation of the skewness $S = T/V^{3/2}$ is formally given by

$$(\Delta S)^2 \simeq \frac{T^2}{V^3}\left[\left(\frac{\Delta T}{T}\right)^2 + \frac{3}{2}\left(\frac{\Delta V}{V}\right)^2\right], \tag{73}$$

when the correlation between the variance and third-order cumulant is neglected. Even though there should be some correlation between V and T, the value of ΔS calculated by the above equation will still be a measure of the error in estimation of the skewness S, because the relative error $\Delta T/T$ will be much larger than $\Delta V/V$.

A4. Poisson case

Since all of the cumulants of the Poisson distribution are equal to the expected value of the stochastic variable, the errors in estimations of the average, variance and third-order cumulant for the Poisson distribution for the expected value of N_{eff} will be approximated by

$$\Delta \overline{X} \simeq (N_{\mathrm{eff}}/N)^{1/2}, \tag{74}$$

$$\Delta V \simeq \left[\left(N_{\rm eff} + 4N_{\rm eff}^2\right)/N\right]^{1/2}, \quad (75)$$

$$\Delta T \simeq \left[\left(N_{\rm eff} + 18N_{\rm eff}^2 + 6N_{\rm eff}^3\right)/N\right]^{1/2}. \quad (76)$$

When $N_{\rm eff}$ is sufficiently large, the relative errors for $\overline{X}$, V, T and the skewness S can be further approximated by $\Delta\overline{X}/\overline{X} \simeq 1/(NN_{\rm eff})^{1/2}$, $\Delta V/V \simeq 2/N^{1/2}$ and $\Delta T/T \simeq \Delta S/S \simeq (6N_{\rm eff}/N)^{1/2}$.

This work has been performed under the approval of the Photon Factory Program Advisory Committee (proposal No. 2009G131).

References

Alexander, L., Klug, H. P. & Kummer, E. (1948). *J. Appl. Phys.* **19**, 742–753.
De Wolff, P. M. (1958). *Appl. Sci. Res.* **7**, 102–112.
Dwiggins, C. W. (1975). *Acta Cryst.* A**31**, 146–148.
Ida, T. (2010). *J. Appl. Cryst.* **43**, 1124–1125.
Ida, T., Goto, T. & Hibino, H. (2009). *J. Appl. Cryst.* **42**, 597–606.
Ida, T. & Hibino, H. (2006). *J. Appl. Cryst.* **39**, 90–100.
Ida, T., Shimazaki, S., Hibino, H. & Toraya, H. (2003). *J. Appl. Cryst.* **36**, 1107–1115.
Izumi, F. & Momma, K. (2007). *Solid State Phenom.* **130**, 15–20.
Langford, J. I., Louër, D. & Scardi, P. (2000). *J. Appl. Cryst.* **33**, 964–974.
Popa, N. C. & Balzar, D. (2002). *J. Appl. Cryst.* **35**, 338–346.